Proceedings of the 5th International Symposium on Steel Science (ISSS 2017)
Nov. 13-16, 2017, Kyoto, Japan: The Iron and Steel Institute of Japan

Transformation mechanism of diffusional reversion from lath martensite to austenite

Nobuo Nakada[1*], Toshihiro Tsuchiyama[2,3], Setsuo Takaki[2,3]

[1] Department of Materials Science and Engineering, Tokyo Institute of Technology,
4259, Nagatsuta-cho, Midori-ku, Yokohama 226-8503, Japan.
[2] Department of Materials Science and Engineering, Kyushu University,
744, Moto-oka, Nishi-ku, Fukuoka 819-0395, Japan.
[3] International Institute for Carbon-Neutral Energy Research (WPI-I^{2}CNER), Kyushu University,
744, Moto-oka, Nishi-ku, Fukuoka 819-0395, Japan.

Abstract: Two characteristics of the diffusional reverse transformation from lath martensite to austenite: (1) lath boundary acts as preferential nucleation site for the austenite reversion, even though it is the boundary with low misorientation angle. (2) the reversed austenite grains nucleated at the lath boundaries have the same orientation as original austenite matrix, were investigated in an ultralow carbon Fe-13%Cr-6%Ni alloy. It was demonstrated that the orientation of reversed austenite grains nucleated at lath boundary is limited so as to be identical by not only a specific orientation relationship with respect to lath structure of martensite matrix but also the internal residual stress in the martensite. Furthermore, it was clarified that the austenite formation at lath boundary reduces the increase in elastic strain energy generated by the austenite nucleation more effectively compared with the case when the reversed austenite grain nucleates at prior austenite grain boundary with high misorientation angle, which leads to the preferential austenite nucleation at lath boundary under the variant restriction.

1. INTRODUCTION

For the improvement of the strength-ductility balance in high strength steels, it is one of useful techniques to finely distribute ductile austenite grains as second phase within martensite matrix. Because, second phase austenite grains contribute to an enhancement of strain hardenability due to deformation-induced transformation as well as its own high strain hardenability. In order to obtain the austenite grains thermally stabilized by the concentration of substitutional austenite-former elements in alloy steels, e.g. 9%Ni steel and medium Mn steel, intercritical annealing to promote reverse transformation from lath martensite to austenite is appropriate, because the austenite growth is controlled by relatively fast diffusion of the elements in martensite matrix [1]. It is interesting that the austenite formed via the diffusional reverse transformation has two characteristics: (1) lath boundary acts as preferential nucleation site for the austenite reversion, even though it is the boundary with low misorientation angle. (2) the reversed austenite grains nucleated at the lath boundaries have the same orientation as original austenite matrix. Since the reversed austenite grains have the same orientation, their growth results in a reconstruction of original austenite structure, which is a well-known phenomenon as “austenite memory” in carbon steels [2-6]. Austenite memory has been discussed on the basis of possible mechanisms, martensitic reversion mechanism [7,8], variant restriction mechanism [9], and retained austenite mechanism [5,6], but it has remained unclear which mechanism is dominant.

In this article, in order to discuss austenite memory basically, the two characteristics of diffusional austenite reversion were investigated individually using an ultralow carbon Fe-13%Cr-6%Ni alloy.

2. EXPERIMENTAL PROCEDURE

The material used in this study is an ultralow carbon martensitic stainless steel (Fe-13%Cr-6%Ni-0.012%C-0.012%N-2.1%Mo alloy in mass%). To obtain lath martensitic single structure, the material was water-quenched after the solution treatment at 1173 K for 1.8ks in austenite single phase region, and then subjected to intercritical annealing at 873, 913, and 953 K in ferrite and austenite two phase region to precipitate austenite. Since T_0 temperature was calculated to be 915 K, austenite never forms

* Corresponding author. E-mail: nakada.n.aa@m.titech.ac.jp, telephone: +81 45 924 5622.

via martensitic reversion during intercritical annealing below the temperature. This material is appropriate for the investigation of the crystallographic analysis of reversed austenite due to the following reasons:
(1) Fully lath martensitic single structure is easily obtained by water-quenching because of its high hardenability. *M*s temperature of this material is around 500 K and austenite has not retained at all after water-quenching treatment (no possibility of the retained austenite mechanism) [10].
(2) Cementite hardly forms on heating of intercritical annealing due to its ultralow carbon content and Cr addition. If cementite or the other kinds of carbide form, its volume fraction is negligible small (no possibility of the variant restriction mechanism under the existence of cementite).
(3) Reversed austenite can retain stably at ambient temperature because Ni enriches into the reversed austenite during intercritical annealing [11].
(4) Two phase region of ferrite and austenite becomes wider at lower temperature by Ni addition, thus just nucleated small austenite grains can be observed in the specimens annealed at a low temperature around 900 K.
Microstructure was observed with optical, scanning electron, and transmission electron microscopies (OM, SEM, and TEM, respectively). Crystallographic characterization was also carried out by means of electron back scatter diffraction (EBSD) method using SEM. Measurement of austenite fraction was performed by thermodilatometry, X-ray diffractometry with CoKα radiation and saturation-magnetization measurement [12]. Stress loading during intercritical annealing was also attempted to investigate the effect of external stress on the reversion behaviour with a Lever-type creep testing machine for test pieces with the gauge section of φ3mm×10mm. The generation of elastic strain energy by formation of an austenite nucleus was simulated by using the general-produced finite element (FEM) method analysis *MARC2005*. Two-dimensional analysis was carried out on the section perpendicular to the close packed direction of martensite and austenite. In the simulation, the shape of austenite nucleus formed at a grain boundary was estimated by the geometrical construction proposed by Lee and Aaronson [13].

3. RESULTS AND DISCUSSION

3.1. Variant restriction of diffusional reversion from lath martensite to austenite [14]

Fig. 1 shows inverse pole figure maps of (a,c) fcc + bcc and (b,d) fcc in Fe-13%Cr-6%Ni alloy isothermally annealed at 913 K for 1.8 ks. The magnified maps (c,d) correspond to the square area A in the maps (a,b), respectively. In EBSD maps, solid lines and broken lines indicate prior austenite grain boundaries and packet boundaries, respectively. These maps reveal the fact that the reversed austenite grains are uniformly distributed within martensite matrix with 0.15 in fraction. In addition, it was confirmed by TEM observation that fine reversed austenite grains thermally stabilized by Ni concentration precipitate on lath boundaries of martensite matrix with acicular shape. It should be noted here that most of reversed austenite grains have a same crystal orientation within one prior austenite grain, as shown by green in the map (b) (Variant 1; V1). The orientation analysis of prior austenite using reconstruction technique assuming Kurdjumov-Sachs (K-S) relationship, $(111)_\gamma//(011)_{\alpha'}$ and $[\bar{1}01]_\gamma//[\bar{1}\bar{1}1]_{\alpha'}$, between austenite and martensite reveals that the

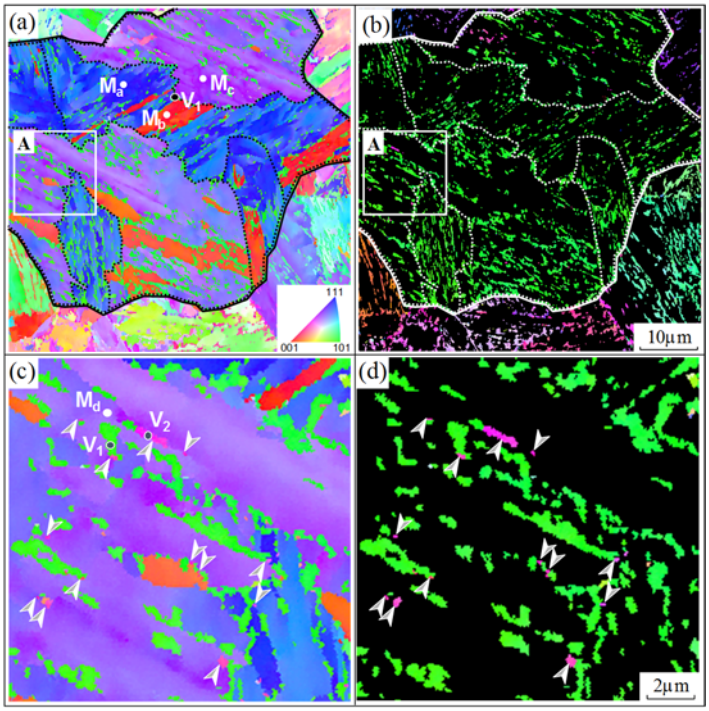

Fig. 1 Orientation imaging maps of Fe-13Cr-6Ni alloy partially isothermally annealed at 913 K for 1.8 ks. Maps (a) and (c) show the martensite matrix and reversed austenite, whereas (b) and (d) show the reversed austenite only.

reversed V1 austenite has the same orientation as the original austenite grain which had existed before water-quenching. That is, austenite memory was realized in this material. On the other hand, it is more interesting in this figure that a small amount of austenite grains has a different orientation as shown by pink in the map (d) (Variant 2; V2), which demonstrates that the austenite grains are not retained austenite but newly formed austenite by intercritical annealing.

Fig. 2 represents the result of orientation analysis for the reversed V2 austenite. The orientations of V1 austenite, V2 austenite, and the martensite block surrounding these austenite (Md in Fig.1 (c)) are shown in the pole figure. It is found that $(111)_{V2}$ is almost parallel with $(111)_{V1}$ and $(011)_{Md}$, and besides, $(\bar{1}10)_{V2}$ is almost parallel with $(0\bar{1}1)_{V1}$ and $(\bar{1}\bar{1}1)_{Md}$. This result indicates that V2 austenite also has K-S relationship with tempered martensite matrix as well as V1 austenite, where the habit plane and the close packed direction correspond to $(011)_{\alpha'}$ and $[\bar{1}\bar{1}1]_{\alpha'}$, respectively. In this case, a twin relationship holds between V1 and V2 austenite on the habit plane of martensite matrix ($(111)\gamma//(011)\alpha'$). The reason why the orientation of reversed austenite formed within martensite matrix is restricted into just two types can be explained in terms of crystallography taking into account a lath morphology, as schematically shown in **Fig. 3**. Assuming that austenite nucleates while holding K-S relationship with respect to martensite matrix, 24 K-S variants of austenite might form on the reversion from bcc to fcc. In the case of grain boundary precipitation, however, the variant of austenite is determined depending on the grain boundary plane: One of the close packed planes, that is nearly parallel to the grain boundary plane, is selected as the habit plane to reduce the activation energy for nucleation [13,15,16]. Lath boundary plane (terrace of martensite lath) is closely $\{011\}_{\alpha'}$ plane [17-20] and act as the habit plane for the nucleation of austenite. This means that one of $\{111\}_{\gamma}$ plane should be parallel to this lath boundary plane. As a result, due to this strong habit plane restriction, the austenite variants are limited to four (Variant 1-4 in Fig. 3) within one martensite block. In addition, on the growth of austenite on the lath boundary plane, the α'/γ interfacial energy can be minimized when austenite grows as one of close packed directions $<011>_{\gamma}$ becomes parallel to one of $<111>_{\alpha'}$; longitudinal direction of martensite lath [19,20]. By adding this growth direction restriction to the habit plane restriction, the possibility of austenite variants is limited to Variant 1 and 2 within one martensite block. These two variants are in twin relationship on the habit plane ($(111)_{\gamma}//(011)_{\alpha'}$). In fact, the above experimental results agree well with this relationship.

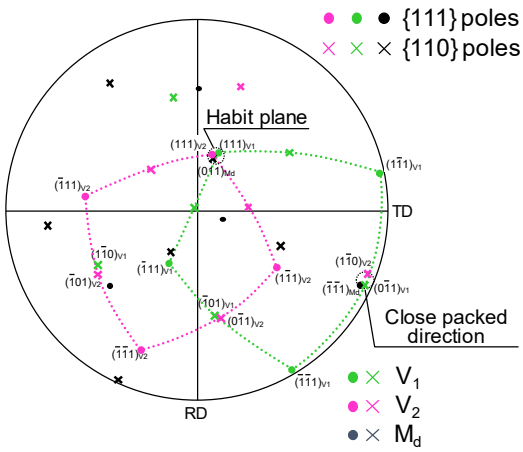

Fig. 2 Pole figure for variant 1 austenite (V1), variant 2 austenite (V2) and the martensite block (Md) surrounding these austenite grains shown in fig. 1 (c).

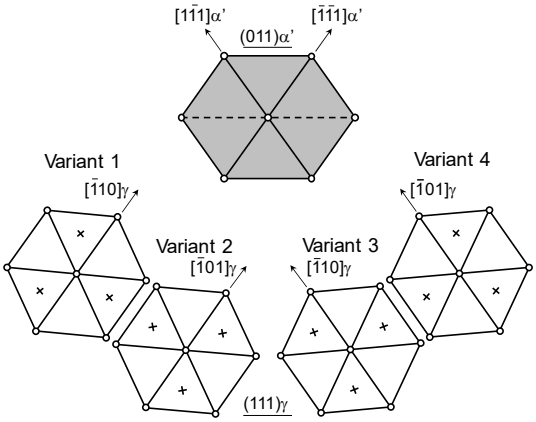

Fig. 3 Schematic showing austenite variants possible on a $(110)_{\alpha'}$ habit plane under the K-S relationship.

The variant restriction mechanism mentioned above predicts the possibility of two variants in a martensite packet and five variants in a prior austenite grain for the diffusional reversion. However, most of reversed austenite grains had the same orientation as that of original austenite (V1). This indicates that there is something promoting the formation of V1 austenite, which cannot be explained only by the crystallographic orientation relationship. In the martensitic transformation, martensite blocks and packets with different crystallographic orientation are introduced to minimize the transformation strain and this results in the formation of the stratified martensitic structure; prior austenite grain, packet, block and lath. However, it is reported that large internal stress remains within

the martensite matrix [21,22]. In terms of stress relief, reversion of martensite to original austenite should be most favourable. To demonstrate the validity of this idea, stress loading reversion was attempted as follows. **Fig. 4** represents the crystal orientation imaging maps of the specimen subjected to partial reversion at 913 K for 0.9 ks under the tensile stress loading of 100 MPa. Since the yield strength of this steel is approximately 240 MPa at 913 K, the applied stress is less than a half of the yield stress. Prior austenite grain boundaries and packet boundaries are drawn by solid line and broken line, respectively. Unlike the result of Fig. 1, not only V_1 austenite but also the other four variants of reversed austenite appear within each prior austenite grain. This means that the austenite memory is disturbed by external stress loading. Careful observation indicates that the variants of reversed austenite are limited to two kinds at a maximum within a packet. The effect of stress loading on area fraction of V1 and V2 austenite is listed in **Table 1**. The area fraction of V2 austenite is markedly increased by applying external stress. This result indirectly demonstrates that the internal local residual stress promotes the formation of V1 austenite during reversion.

From these results, it is concluded that the variant restriction mechanism is reasonable for the austenite memory in ultralow carbon martensite as well as a steel containing cementite. The existence of cementite will give another regulation on diffusional phase transformation, thus the austenite memory should be easy to appear in steels containing cementite than ultralow carbon martensite. However, it should be noted that, in the case of martensitic steels, internal residual stress plays an important role on the appearance of austenite memory.

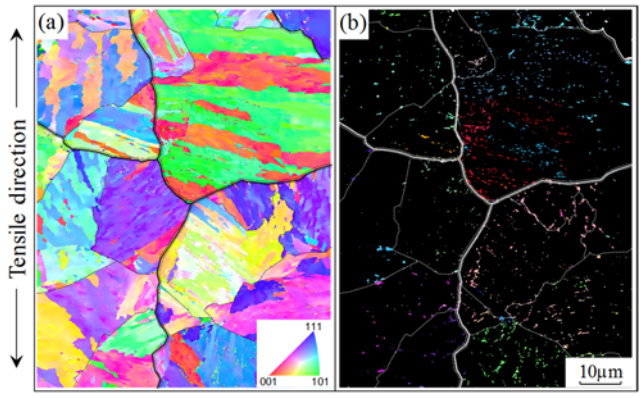

Fig. 4 Orientation imaging maps of Fe-13Cr-6Ni alloy subjected to intercritical annealing at 913 K for 0.9 ks under a uniaxial tensile stress of 100 MPa.
(a) Martensite matrix and reversed austenite.
(b) Reversed austenite shown only.

Table 1 Effect of loading stress on variant selection in the reversion of austenite from lath martensite.

		Area fraction (%)	
		Variant1 (prior γ)	Variant2 (twined relation)
Without loading	Grain1	99	1
	Grain2	96	4
100MPa stress loading	Grain1	50	50
	Grain2	65	35
	Grain3	62	38

3.2. Change in austenite nucleation site depending on reversion temperature [23]

Reversed austenite grains preferentially nucleated at lath boundaries (LBs) within lath martensite matrix, as show in Fig. 1. However, it was found that the nucleation of reversed austenite took place at prior austenite grain boundaries (PAGBs) more frequently with granular shape as intercritical annealing temperature increased, which agrees well with the previous research [9]. From the microstructural characterization by EBSD, the change in the number fraction of austenite grains formed at PAGBs is indicated in **Fig. 5** as a function of intercritical annealing temperature. Only a few percent of austenite have formed at PAGBs in the lower temperature region. However, the austenite at PAGBs is rapidly increased with increasing the temperature, and reaches approximately 40% at 953 K. This result demonstrates that the nucleation site of reversed austenite is changed from LBs to PAGBs by increasing the reversion temperature.

According to the classical nucleation theory, the activation energy for second phase nucleation in phase transformation, ΔG^*, is given by the following equation [16]†1:

$$\Delta G^* = \frac{-1}{4(\Delta Gv + \Delta Gs)} \frac{E^2}{A} \quad \text{[J]} \ \ldots\ldots(1)$$

$\Delta Gv<0$, $\Delta Gs>0$, $\Delta Gv + \Delta Gs<0$

where E, A, ΔG_v, and ΔG_s are the change in interfacial energy, the area of the critical nucleus, the change in chemical free energy, and the change in strain energy per unit area, respectively. This equation means that the frequency of nucleation should be affected by three factors of E, A, and ΔG_s when ΔG_v, i.e. temperature, is constant. In the following paragraph, these three factors, particularly E and ΔG_s, are compared between the cases of nucleation at LB and PAGB to explain the temperature dependence of austenite nucleation site in lath martensite.

In order to estimate the change in interfacial and strain energies by austenite nucleation at LB and PAGB, it is necessary to determine the conditions of both grain boundaries and nuclei. As a model, <111> symmetrical tilt grain boundaries were selected for calculation of representative LB and PAGB. The misorientation angles of these boundaries were set at 2 and 20 degrees, respectively. The grain boundary model for LB is actually valid because it is reported that LB (terrace plane of martensite lath) and longitudinal direction of martensite lath is closely $\{011\}_{\alpha'}$ and $<111>_{\alpha'}$, respectively [17-20]. Meanwhile, the PAGB model is a certain case in which the grain boundary energy becomes maximum. Under the above assumption, the grain boundary energies of LB and PAGB are estimated to be 0.2 and 1.1 J/m^2, respectively, from the result reported by Wolf [24]. According to the two-dimensional construction method proposed by Lee and Aaronson [13], the shape of a critical nuclei of austenite formed at LB and PAGB are expected to have an ideal shape minimizing the activation energy for nucleation, as drawn in **fig. 6**. This is a geometric drawing method using two circles with radius r, whose radius and the distance between the centers are proportional to the incoherent interfacial and grain boundary energies, respectively. In this study, grain boundary energies of 0.2 and 1.1 J/m^2 mentioned above were used for LB and PAGB. In addition, interfacial energies of 1.0 and 0.2 J/m^2 were applied to the incoherent α'/γ interface and the coherent α'/γ interface with K-S relationship [25]. Since an austenite formed at LB generally has the same orientation as that of a prior austenite grain, the α'/γ interface of austenite nucleus at LB should be coherent interface having K-S relationship with matrix on both sides (a). On

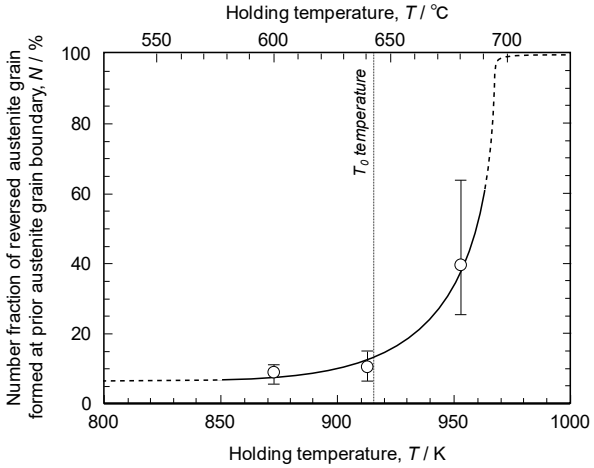

Fig. 5 Change in the number fraction of austenite grains formed at prior austenite grain boundaries.

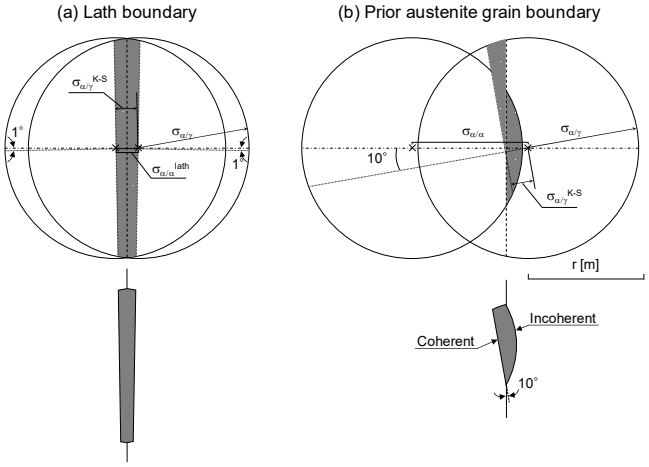

Fig. 6 Shape of a critical nuclei of austenite formed at (a) lath boundary and (b) prior austenite grain boundary.

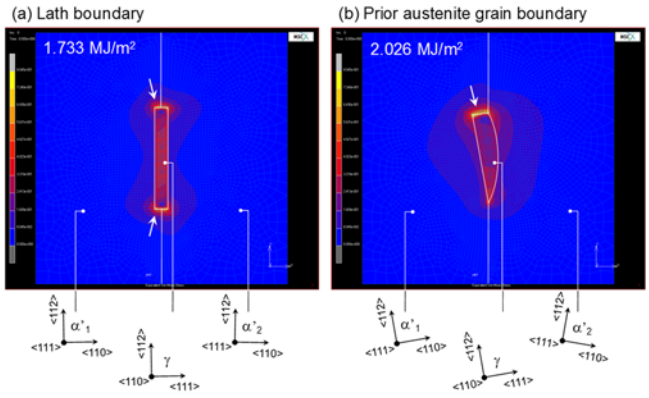

Fig. 7 Result of FEM analysis showing the elastic strain distribution generated by austenite nucleation at (a) lath boundary and (b) prior austenite grain boundary.

the other hand, an austenite nucleus formed at PAGB can hold K-S relationship only with either side of matrix due to crystallographic geometry. Therefore, its shape necessarily becomes granular-type surrounded by both coherent and incoherent interfaces. In such case, the misorientation angle between the coherent interface and PAGB should be 10 degrees (b), because the activation energy for austenite nucleation could be minimized by selecting a close packed plane which is nearly parallel to the PAGB as the facet interface. The expected shapes of austenite nuclei at LB and PAGB basically correspond to the experimental results observed by TEM. From these results, the volume of critical nucleus and the change in interfacial energy by austenite nucleation at LB and PAGB can be calculated, as shown in **Table 2**. This calculation indicates that the austenite nucleation at LB leads to a larger increment of interfacial energy than the case of PAGB, mainly because a part of PAGB is disappeared by austenite nucleation. Consequently, it is understood that PAGB is more advantageous than LB for austenite nucleation from the view point of interfacial energy.

Table 2 Volume of critical nucleus and change in interfacial energy by austenite nucleation at (a) lath boundary and (b) prior austenite grain boundary.

	Change of interfacial energy, E / J	Volume of the critical nucleus, v / m^2
(a) Lath boundary	0.744 r	0.392 r^2
(b) Prior austenite boundary	0.399 r	0.191 r^2

Since the martensite matrix and the reversed austenite have differences in density, thermal expansion, shear modules and so on, transformation strain should be generated though the nucleation of austenite. The generation of strain energy works as a resistance to phase transformation, and thus, the nucleation site would be selected such that the increase in strain energy is minimized. To estimate the change in strain energy caused by formation of an austenite nucleus, FEM analysis was carried out for the austenite nucleation at LB and PAGB. In this analysis, the increase in elastic strain energy was calculated on the assumption that the elastic transformation strain is never accommodated by plastic deformation and atomic diffusion at interface, that is, the calculation result would give a solution of maximum possible strain energy distribution. **Fig. 7** is the result of FEM analysis showing the strain energy distribution caused by an austenite nucleus. The crystal orientation condition and nucleus shape (see fig. 6) in respective cases are again applied here. In the case of LB (a), the left side of facet interfaces was fixed to be a perfect habit plane. For lattice parameters used for martensite and austenite were 0.286 and 0.351 nm, respectively [26]. In addition, the anisotropies of shear modulus in both phases were considered by using the data of pure iron and austenitic stainless steel [27]. This result demonstrates that the local strain is concentrated more effectively at the incoherent α'/γ interfaces as indicated by the white arrows. Additionally, the elastic strain in martensite matrix is more widely expanded in the case of PAGB (b) than that of LB (a). Comparing of the total increment of strain energy per unit area between both cases reveals that austenite nucleation at PAGB (b) generates 1.17 (2.026/1.733) times larger total increments of strain energy than the case of LB (a). It is concluded that LB is more advantageous than PAGB for austenite nucleation from the view point of strain energy, which is the opposite tendency of the interfacial energy calculation mentioned in the previous section.

From above calculations, temperature dependence of austenite nucleation site in lath martensite can be explained as follows. When the value of ΔG_s for LB (see eq. [1]) is g J/m^2, the substitution of the results of Table 2 and Fig. 8 into eq. [1] gives ΔG^* for LB and PAGB as follows:

$$\Delta G^*_{LB} = \frac{-0.353}{\Delta Gv + g} \quad \text{[J] ……[2]}$$

$$\Delta G^*_{PAGB} = \frac{-0.208}{\Delta Gv + 1.17g} \quad \text{[J] ……[3]}$$

Here, ΔG_v (<0) is the change in chemical free energy, and this is decreased (the absolute value is increased) with rising reversion temperature. **Fig. 8** shows the difference between ΔG^*_{LB} and ΔG^*_{PAGB} (ΔG^*_{LB} - ΔG^*_{PAGB}) as a function of ΔG_v. The difference in ΔG^* is decreased with increasing ΔG_v, and then changed from positive to negative at -1.41g J/m^2. This means that austenite tends to nucleate at LB when the reversion temperature is sufficiently lowered to have the driving force (ΔG_v) be comparable to

ΔG_s in magnitude. On the other hand, when the driving force is much larger than ΔG_s at a higher reversion temperature, the preferential nucleation site would change from LB to PAGB due to the decline of the effect of ΔG_s. It is obvious that the above calculation models for interfacial and strain energies lack some important effects to be considered. For example, we should pay attention to the fact that the elastic strain energy could be accommodated by an atomic diffusion and an introduction of misfit dislocations. The PAGB nucleus with another grain boundary character should result in somewhat different energy generation. More basically, the two-dimensional calculation is just a simplified estimation. We need further consideration and study on nucleation behavior in order to make more rigorous model. However, the calculation demonstrates that elastic strain energy acts as a very important role for the austenite reversion from lath martensite, which agree well with the loosening of austenite variant restriction under the loading of external stress, as shown in Fig.4 and Table 2. Furthermore, one of authors reported that large elastic strain energy, approximately 1000 J/mol, remains in iron martensite [22].

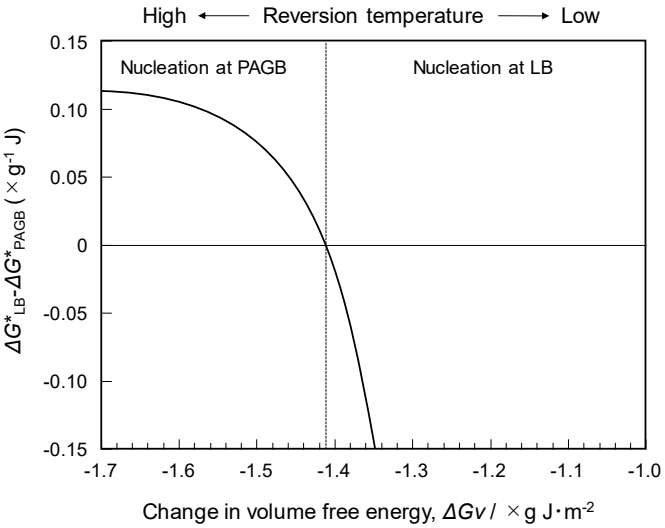

Fig. 8 Difference between activation energies at lath boundary and prior austenite grain boundary as a function of change in volume free energy.

†1: In this study, activation energy for second phase nucleation was written as a quadratic function of E for two-dimensional analysis of interfacial and strain energies.

4. CONCLUSIONS

In order to discuss austenite memory basically, the two characteristics of diffusional austenite reversion were investigated individually using an ultralow carbon Fe-13%Cr-6%Ni alloy. The results obtained are summarized as follows:

1. Reversed austenite grains are formed along lath boundaries as well as block boundaries and packet boundaries. Most of the reversed austenite grains within a prior austenite grain have a same crystallographic orientation. However, some austenite grains have a different orientation in twin relationship with the major reversed austenite grains.
2. All of the reversed austenite grains have the Kurdjumov-Sachs relationship to the martensite matrix, and the kinds of austenite variant are theoretically predicted as follows by taking into consideration the crystallographic relations among the habit plane, the close packed direction of austenite and martensite lath boundary; two kinds of variant in twin relation within a packet and five kinds of variant within a prior austenite grain.
3. It was suggested that internal local residual stress plays an important role on the appearance of austenite memory, that is, the reversion of martensite to austenite with the same crystallographic orientation as that of original austenite. And also it was confirmed that, under the loading of external stress, the austenite memory is confused and the other four variants of austenite appears frequently.
4. The shape and nucleation site of reversed austenite are changed depending on reversion temperature. In a lower temperature of austenite and ferrite two-phase region, acicular austenite grains are frequently formed at the lath boundaries. On the other hand, in higher temperature, granular ones are mainly formed at the prior austenite grain boundary.
5. The temperature dependence of austenite nucleation site in lath martensite is essentially explained by the classical nucleation theory considering the change in interfacial energy and elastic strain energy. Austenite tends to nucleate at lath boundary when the reversion temperature is sufficiently lowered to have the change in chemical free energy be comparable to the change in strain energy in magnitude.

REFERENCES

[1] N. Nakada, K. Mizutani, T. Tsuchiyama and S. Takaki: *Acta Mater.*, **65**(2014), 251-258.
[2] M. Baeyertz : *Trans. ASM*, **30**(1942), 458-490.
[3] R. Honma : *Tetsu-to-Hagane*, **58**(1972), 119-127.
[4] V. D. Sadovskii and B. K. Sokolov : Problems of physical metallurgy and heat treatment, Moscow, (1960), 5.
[5] S. T. Kimmins and D. J. Gooch : *Met. Sci.*, **17**(1983), 519-532.
[6] T. Hara, N. Maruyama, Y. Shinohara, H. Asahi, G. Shigesato, M. Sugiyama and T. Koseki: *ISIJ Inter.*, **49**(2009), 1792-1800.
[7] S. S. D'Yachenko and G. V. Fedorov: Fiz. Met. Metalloved., 18(1964), 73-77.
[8] S. Matsuda Y. Okamura: Tetsu-to-Hagane, 60(1974), 226-238.
[9] S. Watanabe and T. Kunitake: Tetsu-to-Hagane, 61(1975), 96-106.
[10] T. Maki and I. Tamura: *Tetsu-to-Hagane*, **67**(1981), 852-866.
[11] N. Nakada, J. Syarif, T. Tsuchiyama and S. Takaki: *Mater. Sci. Eng. A*, **374**(2004), 137-144.
[12] S.Takaki, Y.Tokunaga and K.Tomimura*Tetsu-to-Hagane*, **73**(1987), S539
[13] J. K. Lee and H. I. Aaronson : *Acta Met.*, **23**(1975), 799-808.
[14] N. Nakada, T. Tsuchiyama, S. Takaki and S. Hashizume: *ISIJ Inter.*, **47**(2007), 1527-1532.
[15] P. R. Howell and R. W. K. Honeycombe: *Proceedings of an International Conference on Solid-Solid Phase Transformation*, (1981), 399-419.
[16] J. K. Lee and H. I. Aaronson : *Acta Met.*, **23**(1975), 809-820.
[17] S. Takeuchi, T. Honma and S. Suzuki : *J. Jpn. Inst. Met.*, **21**(1957), 51-55.
[18] A. H. Greninger and A. R. Troiano: *Trans. AIME*, **140**(1940), 307-331.
[19] V. I. Izotov; Phys. *Met. Metallogr.*, **34**(1972), 112
[20] K. Wakasa and C. M. Wayman: *Acta Metall.*, **29**(1981), 973-990.
[21] Z. Cong, Y. Murata, Y. Tsukada and T. Koyama, *Phil. Mag.*, **93**(2013), 1073-1747.
[22] N. Nakada, N. Kusunoki, M. Kajihara and J. Hamada: *Scripta Mater.*, **138**(2017), 105-108.
[23] N. Nakada, T. Tsuchiyama, S. Takaki and N. Miyano: *ISIJ Inter.*, **51**(2011), 299-304.
[24] D. Wolf: *Phil. Mag.*, **62**(1990), 447-464.
[25] S. Takaki and K. Tsuzaki : *Metallograpy*, Asakura Publishing Co., Ltd., Tokyo, (2000), 136.
[26] M. E. Straumanis and D. C. Kim: *Z. Metallk*, **60**(1969), 272-277.
[27] JSME Data Book *The Modulus of Elasticity of Metals and Alloys*, The Japan Society of Mechanical Engineers, Tokyo, (2001)